Journal of Power Sources 262 (2014) 86–92

Contents lists available at ScienceDirect

Journal of Power Sources

journal homepage: www.elsevier.com/locate/jpowsour

Constructing hierarchical fastener-like spheres from anatase TiO_2 nanosheets with exposed {001} facets for high-performance dye-sensitized solar cells

Weiwei Sun [a], Kang Sun [b], Tao Peng [a], Sujian You [a], Haiming Liu [a], Liangliang Liang [a], Shishang Guo [a,*], Xing-Zhong Zhao [a,*]

[a] School of Physics and Technology and Key Laboratory of Artificial Micro- and Nano-structure of Ministry of Education, Wuhan University, Wuhan 430072, China
[b] School of Electrical Engineering and Automation, Henan Polytechnic University, Jiaozuo 454000, China

HIGHLIGHTS

- We reported a facile one-pot approach to prepare TiO_2 HFSs with exposed {001} facets.
- The TiO_2 HFSs exhibit superior light scattering and dye loading amount property.
- This study provides a convenient route for the development of novel hierarchical TiO_2.

GRAPHICAL ABSTRACT

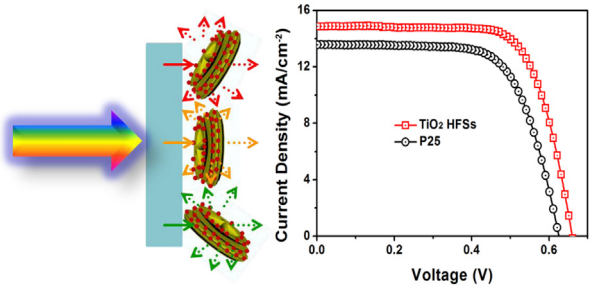

ARTICLE INFO

Article history:
Received 11 January 2014
Received in revised form
19 February 2014
Accepted 19 March 2014
Available online 27 March 2014

Keywords:
Fastener-like
TiO_2 nanosheets
Exposed {001} facets
Excellent light scattering effect
Dye-sensitized solar cells

ABSTRACT

Hierarchical fastener-like spheres assembled from anatase TiO_2 nanosheets with exposed {001} facets are successfully synthesized *via* a facile one-pot hydrothermal process. Compared with standard commercial P25, the as-obtained hierarchical fastener-like TiO_2 spheres exhibit an improved light harvesting efficiency, owing to the excellent light scattering effect of layer-by-layer hierarchical structure and superior dye adsorption capacity of the dominant {001} facets. As a consequence, the photoanode composed of TiO_2 fastener-like sphere scattering layer shows an improved DSSCs conversion efficiency of 7.01% compared to that of commercial P25 (5.78%). The remarkable electrochemical performances of hierarchical fastener-like TiO_2 spheres indicate their promising application as scattering materials for DSSCs.

1. Introduction

Since the pioneering work of dye-sensitized solar cells (DSSCs) was reported by O'Regan and Grätzel, DSSCs have been of considerable interest during the last two decades for their easy fabrication, low cost and high energy conversion efficiency [1,2]. Up to date, the power conversion efficiency of over 12% under 1 sun of illumination makes a new milestone of DSSCs, which incorporates a cobalt complexes based redox mediator in conjunction with zinc porphyrin dye as sensitizer [3]. The photoanode, which is the heart component of DSSCs, is usually fabricated using TiO_2 nanoparticles. As we know, the nano-sized TiO_2 particles in the working electrode

* Corresponding authors. Tel.: +86 27 87642784; fax: +86 27 68752569.
E-mail addresses: gssyhx@whu.edu.cn (S. Guo), xzzhao@whu.edu.cn (X.-Z. Zhao).

http://dx.doi.org/10.1016/j.jpowsour.2014.03.086
0378-7753/

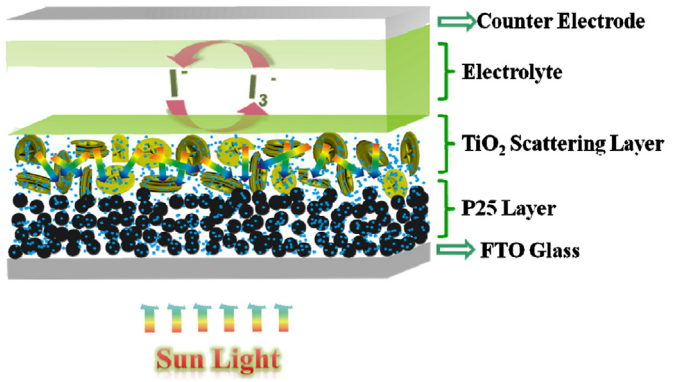

Scheme 1. Schematic representation of the DSSCs photoanode assembled using TiO_2 HFSs as the light scattering layer.

are very weak for visible light scattering effect, which may be result in a considerable portion of the light in the DSSCs transmitting through the certain thickness TiO_2 film without being absorbed by the sensitizer. Moreover, presently most used dyes (typically, N3 or N719), show much reduced light absorption efficiency in the red region [4]. To these ends, much effort has been dedicated to explore new approaches to improve light harvesting efficiency [5,6]. Apart from the new-type sensitizer, it has been demonstrated that incorporating scattering layers into photoanode films can enhance light harvesting efficiency, consequently improve the performance of the solar cells [7,8]. However, the utilization of large size scatterers usually inevitably results in decrease of surface area as well as the dye molecule loading, which counteracts the enhancement effect of light harvesting efficiency [7]. To solve the issue, hierarchically mesoporous microspheres, which are comprised of polydisperse nanosized crystallites aggregates, have been reported as a dual-function scatterers [5,7,9]. These approaches allow the incorporation of sufficient scatterers and thus maintain the high level of dye loading capacity owing to their large internal specific surface area. However, the synthesis process of the hierarchically mesoporous microsphere is usually tedious and hard to manipulate.

Meanwhile, it has been reported that the anatase TiO_2 crystals with exposed {001} facets could adsorb comparatively more dye molecules than the other facets, which is supported by theoretical and experimental results [10–14]. This type of TiO_2 could be advantageous for fabrication of photoanodes for DSSCs applications. Incorporation of large size anatase TiO_2 crystals with exposed {001} facets could, on one hand, serves as effective Mie scatterers, and on the other hand, improves the dye molecules adsorption, both are important attributes for leading to a significant enhancement of the light harvesting capability.

Herein, we report a facile one-pot solvothermal route of synthesizing hierarchical fastener-like spheres, which are layer-by-layer self-assembled from anatase TiO_2 nanosheets with exposed {001} facets. To the best of our knowledge, this is the first time to report these novel hierarchical fastener-like TiO_2 spheres with exposed {001} facets (denoted as TiO_2 HFSs) used as a novel scattering layer for high-efficiency dye-sensitized solar cells, which have been demonstrated to possess tremendous dye absorbed amount as well as admirable light scattering property. When the DSSCs photoanodes assembled using these TiO_2 HFSs as the light scattering top layer and commercial P25 film as the bottom layer, the overall energy conversion efficiency (η) of 7.01% has been achieved, which is 21.3% higher than that of commercial P25 counterparts (5.78%) with the similar thickness. A proposed schematic diagram for the configuration of DSSCs assembled using TiO_2 HFSs as the light scattering layer is shown in Scheme 1.

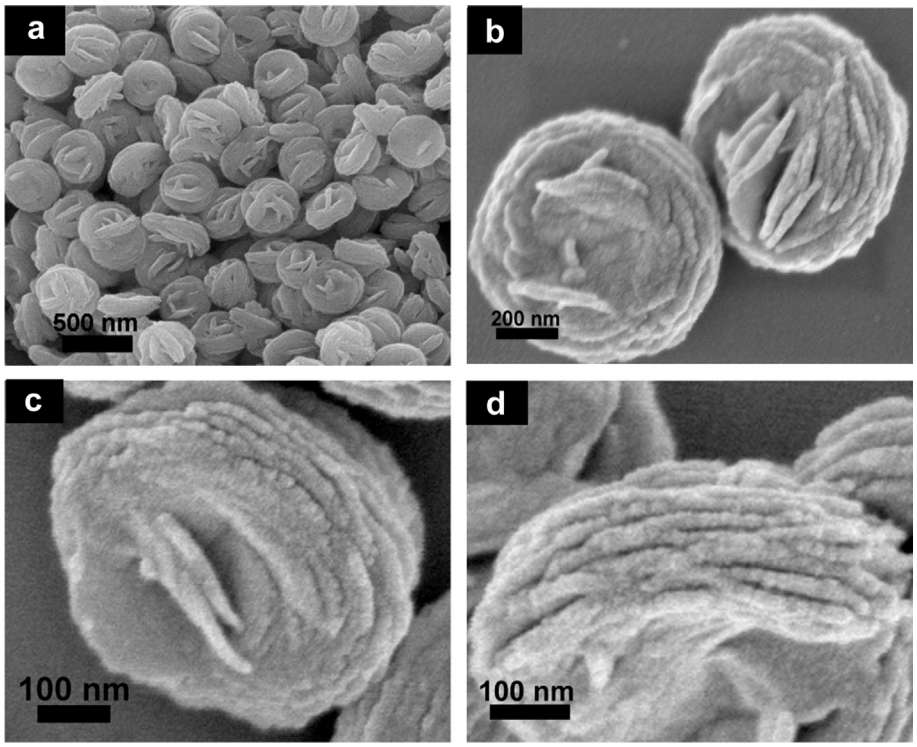

Fig. 1. (a) Low-magnification SEM and (b) high-magnification SEM images of the as-synthesized TiO_2 HFSs; (c) front-view SEM and (d) side-view SEM images of an individual TiO_2 HFS.

2. Experimental

2.1. Material synthesis

Anatase TiO_2 HFSs with exposed {001} facets were prepared by a facile one-step hydrothermal method. In a typical experiment, we mixed titanium tetrafluoride (0.30 g) in 80 mL of solution contained diethylene glycol and benzyl alcohol ($v/v = 1:1$) until obtaining a homogeneous solution under continuous magnetic stirring for about 4 h. Then, the mixed solution was transferred to a Teflon-lined stainless steel autoclave of 100 mL capacity and heated for 12 h at 180 °C. Finally, the white, crystalline titania powder was collected by centrifugation, washed with ethanol and then dried in vacuum at 80 °C.

2.2. Fabrication of DSSCs

For preparation of the TiO_2 HFSs paste, 0.9 g of the prepared TiO_2 HFSs powder was added into the solution containing ethanol (4 mL), water (1 mL), acetylacetone (0.16 mL) and then stirring for 2–3 h. The TiO_2 P25 paste was prepared similar to our recent report [15]. Doctor-blade method was used to prepare photoelectrodes followed by sintering at 500 °C for 30 min. For dye adsorption, the TiO_2 photoanode was immersed in a 0.5 mM N719 ethanol solution and heated at 60 °C for 12 h, then rinsed with ethanol and dried. The liquid electrolyte was prepared by blending 1 M PMII (1-methyl-3-propyl imidazolium iodide), 0.04 M LiI, 0.03 M I_2, 0.1 M GuSCN (guanidinium thiocyanate), 0.5 M TBP(4-*tert*-butylpyridine) in acetonitrile and propylene carbonate ($v/v = 1:1$) between them.

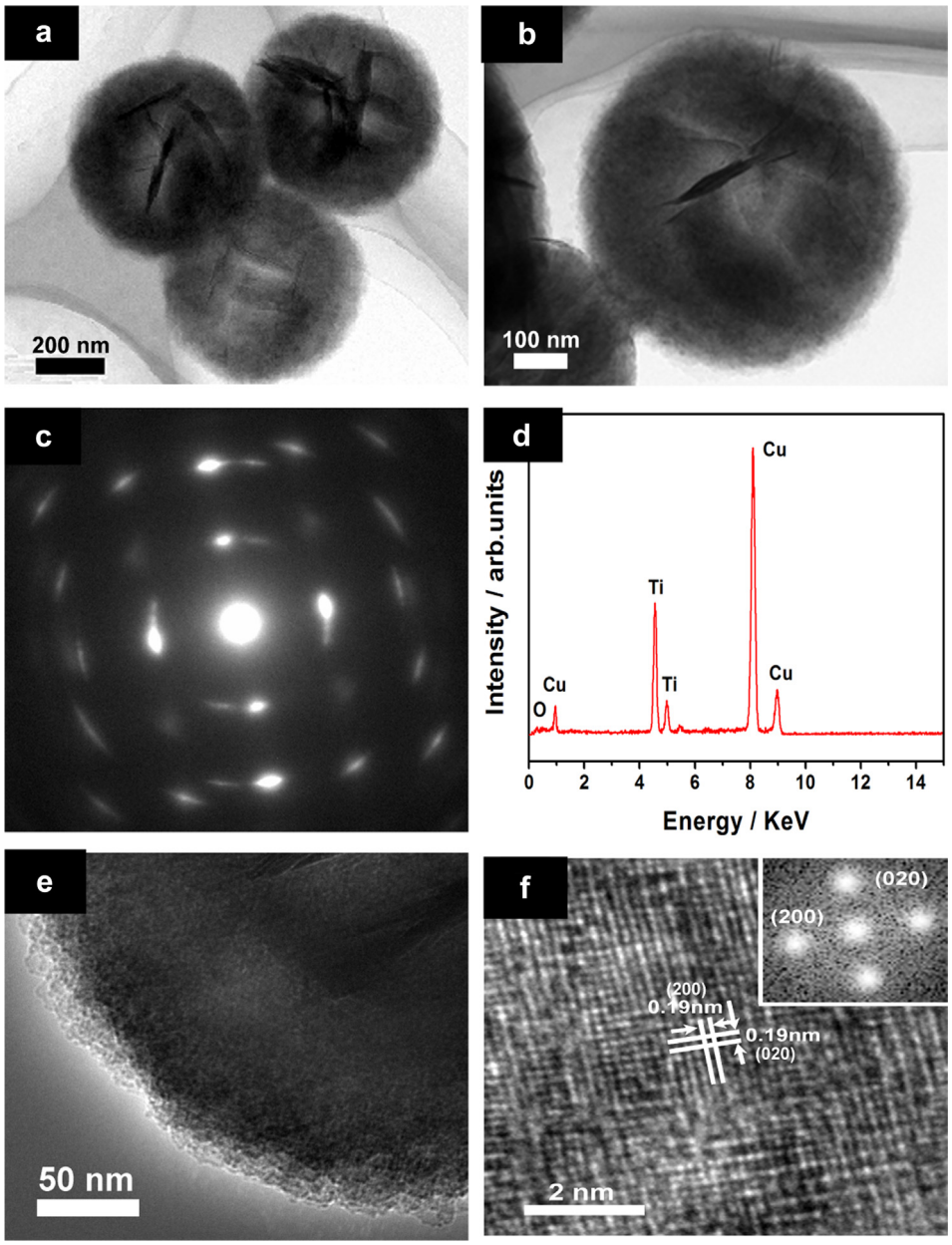

Fig. 2. (a–b) TEM images of as-prepared anatase TiO_2 HFSs; (c) the corresponding SAED pattern recorded from Fig. 2b; (d) EDX analysis of the anatase TiO_2 HFSs; (e) TEM image recorded around the edge of a TiO_2 HFSs; (f) HRTEM image of TiO_2 HFSs showing two sets of perpendicular lattice fringes with a spacing of 0.19 nm (the inset shows the FFT pattern indexed to the [001] zone).

The Pt counter electrode was prepared by depositing a thin layer of Pt on FTO by magnetron sputtering.

2.3. Characterization

X-ray diffraction (XRD) characterization was performed on a D8 Focus diffractometer. Field emission scanning electron microscopy, FE-SEM (Sirion FEG) was applied to study the morphology and structure of the as-prepared samples. TEM and HRTEM investigations were carried out using a JEOL 2010, equipped with an energy dispersive X-ray analysis (EDX) system. The specific surface area and pore size distribution of as-prepared samples were investigated by Brunauer–Emmett–Teller (BET) nitrogen sorption–desorption measurement (JW-BK, China). To obtain the dye loading amount adsorbed on different photoanodes, NaOH aqueous solution (0.1 M) was used for desorption and UV–vis spectrometer (Varian Carry 5000) was used to measure the absorption spectra. Diffuse reflection spectrums of the films were observed on Carry 5000. The incident photon conversion efficiency (IPCE) was measured using a 150 W xenon lamp (Oriel) fitted with a monochromator (Cornerstone 74004) as a monochromatic light source ranging from 400 to 700 nm. The photocurrent–voltage characteristics of the cells were recorded by applying external potential bias to the device under AM 1.5 simulated illumination (Newport, 91192) with a power density of 100 mW cm^{-2}, which was calibrated by a Si photodiode, and the active area was controlled by a 0.25 cm^2 mask. Electrochemical impedance spectroscopy (EIS) measurements were also performed on CHI 660C with the frequency ranging from 100 kHz to 0.1 Hz under the open-circuit voltage in the illumination.

3. Results and discussion

The typical X-ray diffraction (XRD) pattern of as-synthesized TiO_2 HFSs is shown in Fig. S1. All the peaks match the diffraction pattern of anatase TiO_2, which can be well assigned to the pure tetragonal phase anatase structure (JCPDS card no. 21-1272).

The morphology of the as-prepared TiO_2 HFSs was examined by FE-SEM (Fig. 1). As shown in Fig. 1a, numerous of TiO_2 HFSs with diameters ranged from 400 to 500 nm were uniformly distributed. The high magnification SEM image (Fig. 1b) clearly displayed that the as-prepared TiO_2 HFSs were layer-by-layer (LBL) assembled from TiO_2 nanosheets. From the front view of an individual TiO_2 HFS (Fig. 1c), it can be seen that the TiO_2 HFS displayed the hierarchically umbilicate structured. Fig. 1d showed the side-view of an individual TiO_2 HFS, which also demonstrated that the TiO_2 HFSs were LBL self-assembled by well-defined TiO_2 nanosheets. Importantly, this hierarchical structure could significantly enhance the specific surface area and porosity of the as-prepared TiO_2 HFSs, which therefore significantly boost dye absorption and injection efficiency of photo-excited electrons into semiconductors. Moreover, it can be deduced that this sub-micron TiO_2 HFSs could serve as effective scatterers for incident light in the TiO_2 photoanode film.

The detailed structures of the TiO_2 HFSs were characterized by TEM and HRTEM (Fig. 2). Fig. 2a reveals that the entire structure of the architecture is umbilicate fastener-like sphere assembled from LBL closely packed TiO_2 nanosheets. Fig. 2b shows TEM image of an individual TiO_2 HFS. The corresponding electron diffraction (SAED) patterns (Fig. 2c) present well defined spots, which confirm the single crystalline nature of TiO_2 HFS. Further energy-dispersive X-ray analysis (EDX) results confirm the presence of both Ti and O

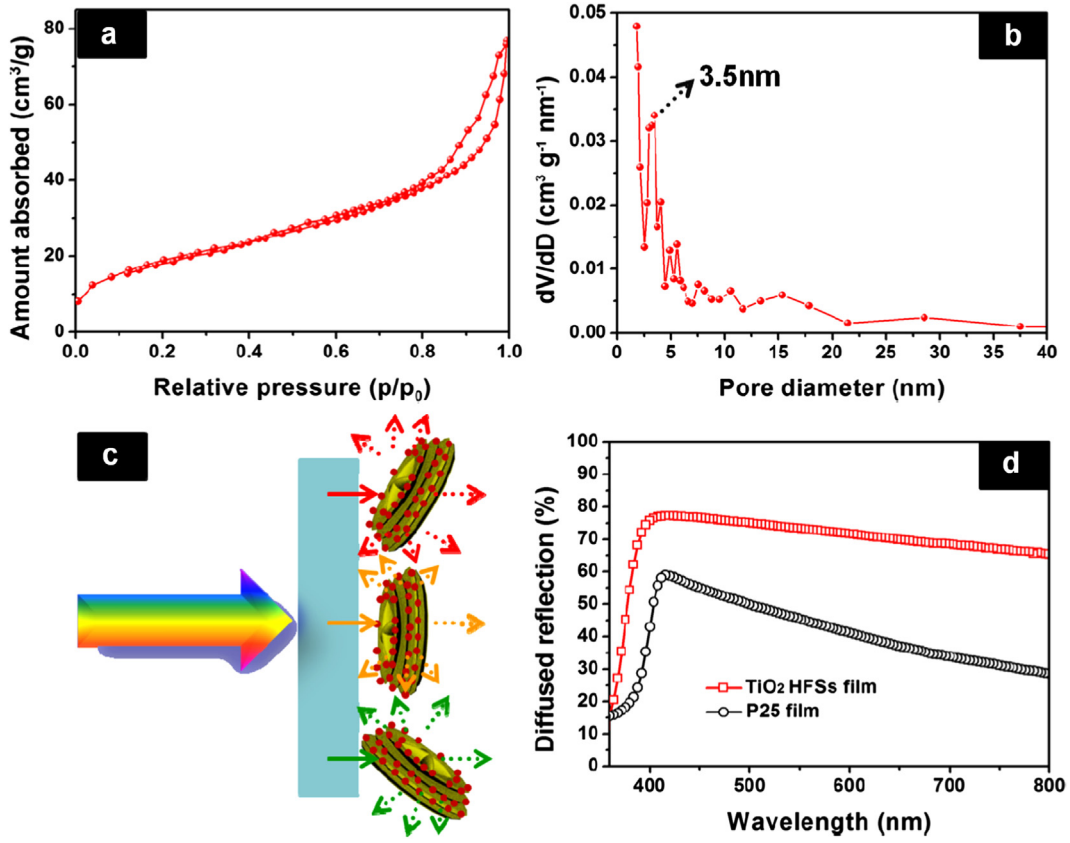

Fig. 3. (a) Nitrogen adsorption–desorption isotherm and (b) Barrett–Joyner–Halenda (BJH) pore size distribution plot of the as-prepared TiO_2 HFSs; (c) Schematic illustration of the multiple reflecting and scattering of light in the TiO_2 HFSs; (d) Diffuse-reflectance spectra of the films of TiO_2 HFSs and P25 with the similar thickness of about 13 μm.

elements in TiO_2 HFSs (Fig. 2d). To further investigate the crystal facets of TiO_2 HFSs, it is reasonable to look into the HR-TEM images of randomly selected TiO_2 HFS, which is shown in Fig. 2e. From the HR-TEM image (Fig. 2f), it evidently shows that two sets of lattices are present and that they are oriented perpendicular to each other with an equal interfringe spacing of 0.19 nm, corresponding to {200} and {020} planes of anatase-type TiO_2 HFSs. The fast Fourier transform (FFT) pattern of the same region (inset of Fig. 2f) can be indexed to diffraction spots of the [001] zone [16]. The results suggest that TiO_2 HFSs LBL assembled by anatase TiO_2 nanosheets have exposed {001} facets. The formation of this LBL hierarchical structure with exposed {001} facets may attribute to the capping effect of fluorine ions and the selective adsorption of diethylene glycol and benzyl alcohol molecules on the surface of TiO_2, which may further acts as a protective capping agent accelerating the LBL self-assembled of TiO_2 nanosheets with exposed {001} facets [17,18].

The porous structure of the TiO_2 HFSs was further investigated with the N_2 adsorption/desorption analysis as shown in Fig. 3a, b. Fig. 3a gives a typical type IV isotherm with an H3 hysteresis loop, indicating a mesoporous structure [16]. The Barrett–Joyner–Halenda (BJH) pore size distribution (Fig. 3b) obtained from the isotherm indicates that the BET surface area of TiO_2 HFSs is about 67.2 $m^2\ g^{-1}$ and shows a distinct salient peak concentrated at about 3.5 nm, which might be attributed to the LBL hierarchical structure of TiO_2 HFSs. It is convincing that the large specific surface area and mesoporous structures of TiO_2 HFSs are in favour of better penetration of electrolyte and more adsorption of the dye molecules when used as scattering layer in DSSCs [19]. The possible reflecting and scattering of light in TiO_2 HFSs photoanode is illustrated in Fig. 3c. It is believed that the micro-sized TiO_2 HFSs can scatter effectively the incident light of different wavelengths in the whole range of visible light. Fig. 3d shows the UV–vis diffuse reflection spectra of the TiO_2 HFSs and P25 photoanodes. The P25 photoanode shows lower diffuse reflectance in the wavelength range between 400 and 450 nm and rapidly decreases as the wavelength increases from 450 to 800 nm due to the small particle size [20]. In contrast, the TiO_2 HFSs photoanode exhibits high diffuse reflectance in the whole visible range regions, which indicates the superior light scattering behaviour of the TiO_2 HFSs photoanode. As a result, the TiO_2 HFSs as bi-functional photoanode materials can not only drastically increase the dye loading rate but also maximize the absorption of light in the range of 400–800 nm, and thus enhance the light harvesting efficiency.

The photocurrent density–voltage (J–V) curves of DSSCs based on TiO_2 HFSs and P25 electrodes were characterized at AM 1.5 irradiation of 100 mW cm^{-2}. For P25 photoanode, ~13.6 μm P25 layer was directly doctor-bladed onto the FTO substrate (Fig. S2a). With regard to TiO_2 HFSs photoanode, ~7.2 μm P25 layer was first doctor-bladed onto the FTO substrate and followed by doctor-blading ~6.6 μm TiO_2 HFSs (Fig. S2b). The typical J–V curves of the two samples are shown in Fig. 4a and detailed parameters of the cells are summarized in Table 1. The DSSCs based on the TiO_2 HFSs reveal an open-circuit voltage (V_{oc}) of 0.66 V, short-current density (J_{sc}) of 14.88 mA cm^{-2} and overall conversion efficiency (η) of 7.01%, whereas DSSCs based on P25 just give a V_{oc} of 0.63 V, J_{sc} of 13.57 mA cm^{-2} and η of 5.78%. As we can seen in Table 1, the amounts of eluted dye for TiO_2 HFSs and P25 photoanodes are 1.28×10^{-7} mol cm^{-2} and 1.07×10^{-7} mol cm^{-2}, respectively, which are calculated by UV–vis absorption spectra of the dyes desorbed from the two different photoanodes (Fig. S3). This enhanced dye adsorption amount of TiO_2 HFSs photoanode can be attributed to the large specific surface area, LBL mesoporous structure and the superior dye adsorption ability of the dominant {001} facets [20]. Therefore, the increase of the J_{sc} could be ascribed

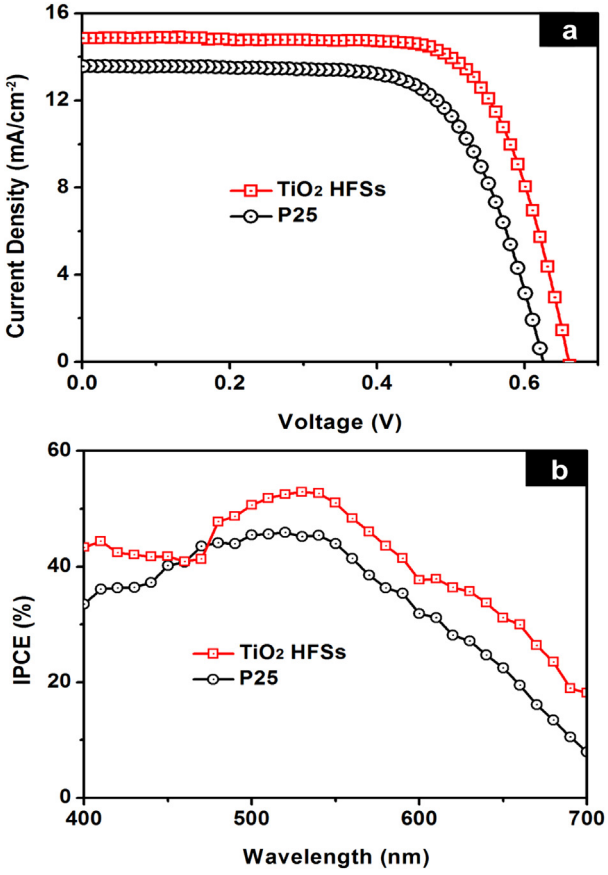

Fig. 4. (a) J–V characteristics and (b) IPCE spectra of the devices with TiO_2 HFSs and P25 photoanodes.

to the effective light-harvesting ability and superior dye adsorption ability. Further, duo to the more compact dye molecule absorption, tri-iodide ions were inhibited to reach the surfaces of TiO_2 HFSs. In other words, direct recombination of excited dye electrons with tri-iodide ion was greatly decreased, which could lead to the higher V_{oc} value of TiO_2 HFSs compared to that of P25. As a result, the overall η of the TiO_2 HFSs is observably 21.3% higher than that of P25 under the same conditions. Fig. 4b displays the incident photo to current efficiency (IPCE) spectra of DSSCs made from TiO_2 HFSs and P25 photoanodes. The IPCE is in good agreement with the η of the solar cells. Compared with the P25 photoanode, the film of TiO_2 HFSs had a higher IPCE over the range from 500 nm to 700 nm. The maximum value of the IPCE spectra appears at about 520–530 nm, and the IPCE of TiO_2 HFSs solar cell is approximately 53%, obviously higher than that of the P25 (46%) solar cell.

Electron transport and recombination properties in DSSCs were investigated using electrochemical impedance spectroscopy (EIS) to further identify the underlying enhancement mechanism and the results were shown in the form of a Nyquist plot (Fig. 5a).

Table 1
Comparison of open circuit voltage (V_{oc}), short-circuit photocurrent density (J_{sc}), fill factor (FF), overall photo-conversion efficiency (η) along with the amount of adsorbed dye N719 for the photoanodes composed of TiO_2 HFSs and P25, respectively.

Electrodes	V_{oc} (V)	J_{sc} (mA cm^{-2})	FF	PCE (%)	Adsorbed dye ($\times 10^{-7}$ mol cm^{-2})
TiO_2 HFSs	0.66	14.88	0.71	7.01	1.28
P25	0.63	13.57	0.69	5.78	1.07

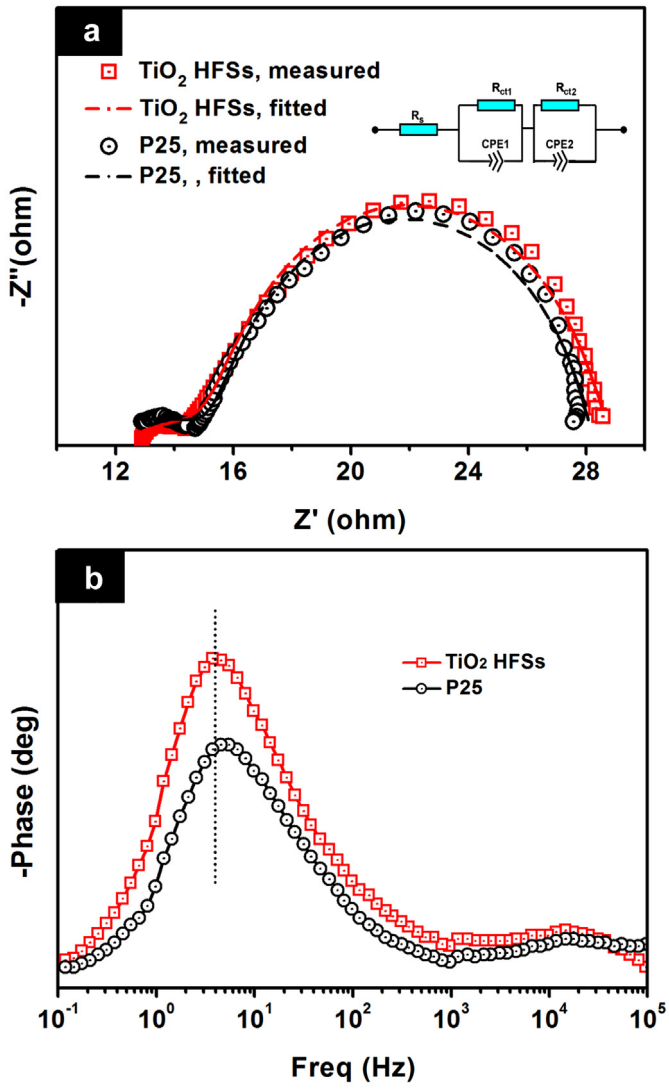

Fig. 5. (a) The Nyquist plots; and (b) the corresponding bode plots of the DSSCs based on TiO_2 HFSs and P25 photoanodes. The inset in (a) displays the equivalent circuit model.

The internal impedances were determined by fitting the experimental data with an equivalent circuit (inset of Fig. 5a), which consists of the total series resistance of the device (R_s), electron transport resistance at the counter electrode/electrolyte (R_{ct1}, the first semicircle in the high frequency region), electron transport and recombination at the photoanode/electrolyte (R_{ct2}, the second semicircles in intermediate frequencies) and the constant phase element of capacitance corresponding to R_{ct1} (CPE1) and R_{ct2} (CPE2), respectively [21–23]. The fitted data determined from EIS analysis are listed in Table 2. The R_{ct1} values of the DSSCs based on TiO_2 HFSs and P25 are 2.13 Ω and 2.83 Ω, respectively. The similar values of R_{ct1} are simply because the identical Pt counter electrode was employed for these two devices. R_{ct2}, associated with the electron transport and recombination at the photoanode/electrolyte, is usually considered to be mainly determined by the charge recombination resistance, with partial contribution from transport resistance [21]. As seen in Table 2, TiO_2 HFSs-based DSSCs shows a higher value of R_{ct2} (14.74 Ω) than that of P25 (13.56 Ω), which implies that electron recombination resistance is increased at the photoanode/electrolyte interface. As mentioned above, this result can be explained by the fact that TiO_2 HFSs are assembled from TiO_2 nanosheets with dominant {001} facets and a "blocking layer" may be formed on the surface of TiO_2 {001} facet due to densely aggregated dye molecules, thereby increasing the recombination resistance as well as the V_{oc} compared to P25. The bode phase plots of EIS spectra, as shown in Fig. 5b, display two main frequency peaks corresponded to the charge transfer process at different interfaces for two kinds of photoanodes. It is found that the maximum frequency peak in the intermediate frequency regime, which is related to electron transfer in the TiO_2 HFSs photoanode, is lower than that of the P25 photoanode. According to the EIS model, the electron lifetime in DSSCs (τ_r) is inversely proportional to the characteristic frequency (f_{max}) of the maximum phase shift in the mid-frequency peak, which could be estimated from the following relationship, $\tau_r = 1/2\pi f_{max}$ [22,23]. As can be seen in Table 2, the characteristic frequencies (f_{max}) at the mid-frequency peaks were 3.74 and 5.49 Hz for TiO_2 HFSs and P25 photoanodes, respectively. So the τ_r for DSSCs with TiO_2 HFSs photoanode was calculated to be 42.55 ms, which was up to 47% longer than that of P25 photoanodes (28.99 ms), implying a lower electron recombination rate. These results suggest that the V_{oc} of TiO_2 HFSs could be heightened compared to P25, because V_{oc} depends logarithmically on the kinetic constant of the back reaction of the injected electron with triiodide and incident photo flux [22], which is in accordance with our previous conclusion. The enhancement can be also explained through that the "blocking layer" may be formed on the surface of TiO_2 HFSs {001} facets aroused by absorbing compact dye molecule. These factors are in favour of achieving higher photoelectric conversion efficiency.

Table 2
EIS parameters of the DSSCs determined by fitting the experimental data to the equivalent circuit model (see Fig. 5a).

Electrodes	R_{ct1} (Ω)	R_{ct2} (Ω)	f_{max} (Hz)	τ_r (ms)
TiO_2 HFSs	2.13	14.74	3.74	42.55
P25	2.83	13.56	5.49	28.99

4. Conclusion

In summary, we have synthesized novel anatase TiO_2 HFSs with dominate {001} facets *via* a one-step hydrothermal process. The as-prepared TiO_2 HFSs exhibit superior scattering effect, admirable dye loading amount property as well as high carriers transfer, which can dramatically improve the photovoltaic performance of DSSCs. A maximum conversion efficiency of 7.01% has been achieved by the DSSCs based on TiO_2 scattering layer, showing 21.3% increment over that derived from DSSCs with commercial P25 photoanode. In addition, the process for synthesis TiO_2 HFSs may provide a convenient route for the development of novel LBL hierarchical TiO_2 photoanodes with exposed {001} facets for clean energy applications.

Acknowledgements

This project was funded by the National Basic Research Program (no. 2011CB933300) of China and the National Science Fund for Talent Training in Basic Science (Grant no J0830310).

Appendix A. Supplementary data

Supplementary data related to this article can be found at http://dx.doi.org/10.1016/j.jpowsour.2014.03.086.

References

[1] B. O'Regan, M. Grätzel, Nature 353 (1991) 737.
[2] M. Grätzel, Nature 414 (2001) 338.
[3] A. Yella, H.-W. Lee, H.N. Tsao, C. Yi, A.K. Chandiran, M.K. Nazeeruddin, E.W.-G. Diau, C.-Y. Yeh, S.M. Zakeeruddin, M. Grätzel, Science 334 (2011) 629.
[4] F. De Angelis, S. Fantacci, E. Mosconi, M.K. Nazeeruddin, M. Grätzel, J. Phys. Chem. C 115 (2011) 8825.
[5] D. Chen, F. Huang, Y.B. Cheng, R.A. Caruso, Adv. Mater. 21 (2009) 2206–2210.
[6] F. Huang, D. Chen, X.L. Zhang, R.A. Caruso, Y.B. Cheng, Adv. Funct. Mater. 20 (2010) 1301.
[7] W.-G. Yang, F.-R. Wan, Q.-W. Chen, J.-J. Li, D.-S. Xu, J. Mater. Chem. 20 (2010) 2870.
[8] K. Zhu, N.R. Neale, A. Miedaner, A.J. Frank, Nano Lett 7 (2007) 69.
[9] Q. Zhang, T.P. Chou, B. Russo, S.A. Jenekhe, G. Cao, Angew. Chem. 120 (2008) 2436.
[10] J. Fan, W. Cai, J. Yu, Chem. Asian J. 6 (2011) 2481.
[11] X. Wu, Z. Chen, G.Q.M. Lu, L. Wang, Adv. Funct. Mater. 21 (2011) 4167.
[12] D. Çakır, O. Gülseren, E. Mete, Ş. Ellialtıoğlu, Phys. Rev. B 80 (2009) 035431.
[13] W.Q. Fang, X.H. Yang, H. Zhu, Z. Li, H. Zhao, X. Yao, H.G. Yang, J. Mater. Chem. 22 (2012) 22082.
[14] R. Hengerer, L. Kavan, P. Krtil, M. Grätzel, J. Electrochem. Soc. 147 (2000) 1467.
[15] N. Huang, B. Sebo, M. Pan, Y. Liu, T. Peng, W. Sun, C. Bu, X. Zhao, Sol. Energy 97 (2013) 266.
[16] J.S. Chen, Y.L. Tan, C.M. Li, Y.L. Cheah, D. Luan, S. Madhavi, F.Y.C. Boey, L.A. Archer, X.W. Lou, J. Am. Chem. Soc. 132 (2010) 6124.
[17] H.G. Yang, C.H. Sun, S.Z. Qiao, J. Zou, G. Liu, S.C. Smith, H.M. Cheng, G.Q. Lu, Nature 453 (2008) 638.
[18] W. Yang, J. Li, Y. Wang, F. Zhu, W. Shi, F. Wan, D. Xu, Chem. Commun. 47 (2011) 1809.
[19] J. Feng, Y. Hong, J. Zhang, P. Wang, Z. Hu, Q. Wang, L. Han, Y. Zhu, J. Mater. Chem. A 2 (2014) 1502–1508.
[20] H. Zhang, Y. Han, X. Liu, P. Liu, H. Yu, S. Zhang, X. Yao, H. Zhao, Chem. Commun. 46 (2010) 8395.
[21] F. Fabregat-Santiago, J. Bisquert, E. Palomares, L. Otero, D. Kuang, S.M. Zakeeruddin, M. Grätzel, J. Phys. Chem. C 111 (2007) 6550.
[22] Q. Wang, J.-E. Moser, M. Grätzel, J. Phys. Chem. B 109 (2005) 14945.
[23] J.T. Park, D.K. Roh, R. Patel, E. Kim, J.H. Kim, J. Mater. Chem. 20 (2010) 8521.